Lithos 304–307 (2018) 95–108

Contents lists available at ScienceDirect

Lithos

journal homepage: www.elsevier.com/locate/lithos

Origin of sapphirine- and garnet-bearing clinopyroxenite xenoliths entrained in the Jiande basalts, SE China

Yan Xiao [a,*], Hong-Fu Zhang [a,b], Zi Liang [a,c], Ben-Xun Su [c,d], Bin Zhu [a], Patrick Asamoah Sakyi [e]

[a] State Key Laboratory of Lithospheric Evolution, Institute of Geology and Geophysics, Chinese Academy of Sciences, Beijing 100029, China
[b] State Key Laboratory of Continental Dynamics, Department of Geology, Northwest University, Xi'an 710069, China
[c] University of Chinese Academy of Sciences, Beijing 100049, China
[d] Key Laboratory of Mineral Resources, Institute of Geology and Geophysics, Chinese Academy of Sciences, Beijing 100029, China
[e] Department of Earth Science, University of Ghana, PO Box LG 58, Legon-Accra, Ghana

ARTICLE INFO

Article history:
Received 15 August 2017
Accepted 3 February 2018
Available online 07 February 2018

Keywords:
Sapphirine
Clinopyroxenite xenolith
Li abundances
Uplift
Lithospheric mantle

ABSTRACT

We present petrological and geochemical data of sapphirine- and garnet-bearing clinopyroxenite xenoliths entrained in the Jiande Cenozoic basalts, SE China, to investigate their igneous and metamorphic history, and reconstruct of the thermal-tectonic evolution of the lithospheric mantle. These xenoliths have an unusual mineral association consisting of clinopyroxene + garnet/kelyphite + spinel (±sapphirine). Clinopyroxene has high Mg# (89–93) and displays convex-upward REE pattern. Garnet, partially to completely kelyphitized, is rich in pyrope end-member. It usually includes relics of spinel, suggesting that garnet was formed at the expense of spinel. The spinel has high MgO (20.8–22.9 wt%) and Al_2O_3 (64.8–67.9 wt%) contents. Sapphirine, forming a rim on spinel, has homogeneous SiO_2 (14.5–14.9 wt%), Al_2O_3 (60.9–61.7 wt%) and MgO (19.7–20.1 wt%) contents, interpreted to be of metamorphic origin. The subsolidus reaction for the formation of sapphirine is as follows: spinel + garnet = sapphirine + clinopyroxene + orthopyroxene. Thus, the earliest mineral assemblage recorded in these xenoliths was spinel + clinopyroxene. The clinopyroxene in the Jiande clinopyroxenite xenoliths has Li abundances (1.04–1.63 ppm) similar to high-P mafic cumulate but much lower than those in crustal eclogite. In addition, the clinopyroxene and garnet do not show positive Eu anomalies. Therefore, the protolith of these three clinopyroxenite xenoliths was most likely a pyroxenite, originating as clinopyroxene + spinel cumulates from mafic melts percolating through the mantle. Many reaction textures such as formation of garnet and sapphirine were developed during decompression possibly coupled with cooling and melt percolation. During this process, the earlier composition of clinopyroxene and spinel also changed. The latest P-T conditions recorded in these xenoliths were at pressure of 8–10 kbar and temperatures of 1069–1094 °C. These observations imply that these rocks have been tectonically uplifted to shallower levels. The uplift process may have been related to lithospheric thinning process accompanied by lithosphere extension and upwelling of the asthenosphere in eastern China.

1. Introduction

Sapphirine is a relatively rare mineral and occurs mostly in Mg- and Al-rich and Ca-poor rocks from several high-temperature granulite terranes, which have been experienced high-grade regional metamorphism (Galli et al., 2011; Jiao et al., 2015; Jiao and Guo, 2011; Lal et al., 1987; Okay, 1994; Santosh et al., 2007, 2009). Sapphirine is commonly associated with orthopyroxene, cordierite and sillimanite. However, experimental studies suggest that sapphirine could be stable under upper-mantle conditions, if appropriate bulk compositions are available (Ackermand et al., 1975). Mantle-derived sapphirine has, to date, been reported the following localities: (1) pyroxenite xenoliths from kimberlites in Stockdale, Kansas (Meyer and Brookins, 1976), (2) basaltic breccia pipes in Delegate, New South Wales, Australia (Griffin and O'Reilly, 1986), (3) basalts in Hannuoba, eastern China (Su et al., 2012), (4) basaltic lavas in Tel Thanoun, Syria rift (Bilal, 2016), (5) garnet clinopyroxenites from the Beni Bousera massif, Morocco (Kornprobst et al., 1990), (6) the Ronda peridotite massif, Spain (Morishita et al., 2001) and (7) the Finero phlogopite-peridotite massif, Italy (Giovanardi et al., 2013). Mantle-derived sapphirine usually coexists with clinopyroxene and has a limited stability field of about 8 to 15 kbar and at 800 to 900 °C in the pyroxenite stability field (Su et al., 2012). Previous studies have shown that sapphirine occurs either as rim on spinel or as elongated lamella intergrowth with clinopyroxene in garnet-clinopyroxene granulite and eclogite

* Corresponding author.
E-mail address: xiaoyan@mail.iggcas.ac.cn (Y. Xiao).

https://doi.org/10.1016/j.lithos.2018.02.004
0024-4937/

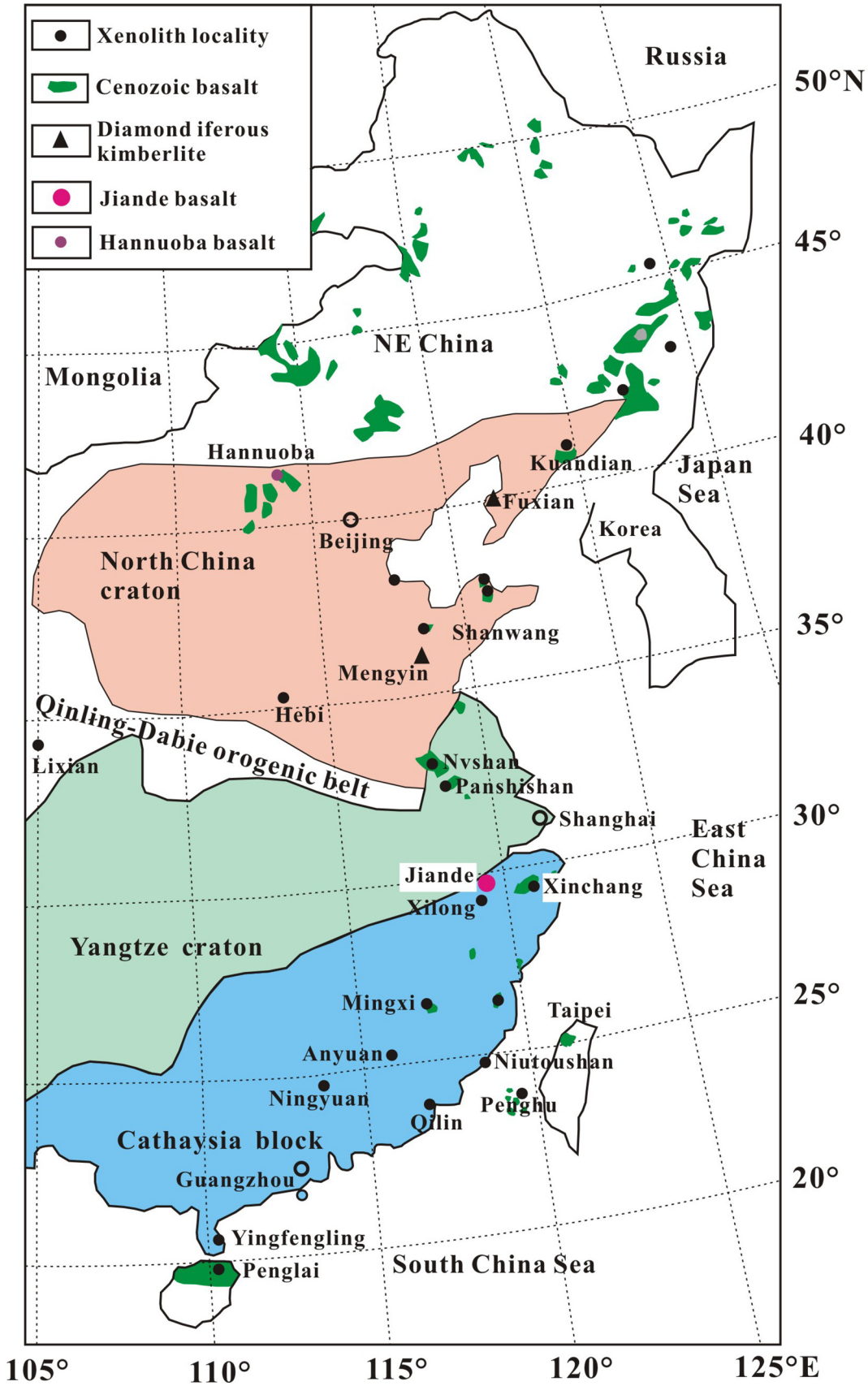

Fig. 1. Simplified geological map showing major tectonic units and xenolith location in eastern China (modified after Huang and Xu, 2010).

xenolith (Griffin and O'Reilly, 1986; Meyer and Brookins, 1976). It also occurs as rim on spinel in spinel pyroxenites (Su et al., 2012; Bilal, 2016).

This paper focuses on newly discovered clinopyroxenite xenoliths from Jiande Cenozoic basalts in Zhejiang Province, SE China. These xenoliths have an unusual mineral association consisting of clinopyroxene + garnet/kelyphite + spinel (±sapphirine). We carry out petrological and geochemical studies for these clinopyroxenite xenoliths, determine their P-T conditions and compare them with other sapphirine-bearing mafic rocks worldwide. These new findings have been used to constrain the origin of sapphirine and the nature of clinopyroxenite, to further constrain their thermal history and possible connection with the evolution of the SE China lithosphere.

2. Geological setting and sample description

Eastern China has been divided into three tectonic blocks, namely; the Xing-Meng Block, the North China Craton and the South China Block. The South China Block consists of two major blocks, with the Yangtze block to the northwest and the Cathaysia block to the southeast (Fig. 1). In the Cathaysia Block, the late Neoproterozoic to Phanerozoic sedimentary rocks and Paleozoic to Mesozoic igneous rocks are widely distributed (Li et al., 2014). Outcrops of pre-Neoproterozoic basement rocks are rare, and the oldest rocks are the Late Paleoproterozoic igneous and metamorphic rocks in the northeastern part of the Cathaysia block (Li et al., 2012; Liu et al., 2009; Xia et al., 2012; Yu et al., 2010). There is no Archean rock exposed in the Cathaysia block, although Archean detrital and/or xenocrystal zircons are founded in various rocks (Li et al., 2014). Cenozoic basaltic rocks are widely distributed from north to south in the Cathaysia block, i.e., the Zhejiang, Fujian, Guangdong and Hainan provinces, and contain a wide variety of deep-seated xenoliths (Zhang and Cong, 1987; Fig. 1). In the Zhejiang Province, Cenozoic volcanism is distributed in the Xinchang, Xilong and Jiande fields and host abundant peridotite xenoliths such as spinel lherzolite and garnet lherzolite (Hao et al., 2014; Liu et al., 2012; Lu et al., 2015; Xiao et al., 2017; Fig. 1). Based on Ar-Ar data, Ho et al. (2003) suggested that the Cenozoic basaltic eruptions in the Zhejiang Province occurred in two stages, namely; (1) 26.4–15.6 Ma, which is mainly composed of basanites and nephelinites, and (2) 10.5–2.5 Ma, which dominantly comprises alkali basalts and tholeiites.

In this study, three scarce clinopyroxenite xenoliths were collected from the Jiande basalts. They are large in size (~15 cm in diameter) and gray-green in color. These xenoliths have a granuloblastic metamorphic texture with clinopyroxene (65–79%), garnet/kelyphite (16–22%) and spinel (5–11.5%) as the major phases, two of which contain sapphirine (0–3%) (Table 1; Figs. 2 and 3).

In two sapphirine-bearing clinopyroxenite xenoliths, clinopyroxene crystal is 3.0–4.0 mm in size and does not show detectable zoning on BSE images. The garnet typically forms large grains and is partially or completely replaced by an extremely fine-grained, symplectitic "kelyphite", consisting of orthopyroxene, plagioclase and spinel (Figs. 2 and 3a-d). The microstructure of kelyphite is characterized by the occurrence of small elongated patches of plagioclase enclosed in much larger crystals of orthopyroxene, and thin vermicular lamellae of spinel (2e, f). Spinel occurs as rounded grain in the kelyphite (or clinopyroxene) or at the contact between the clinopyroxene and kelyphite (Figs. 2b–f and 3b–d). Sapphirine is anhedral and usually occurs as a rim on spinel (Figs. 2b-f and 3b-d). The boundary of sapphirine and spinel is sharp (Fig. 4). Plagioclase is polygonal and occurs as an accessory mineral (0.5%) in one xenolith (Sample SZZ12-09; Table 1 and Fig. 3b).

The mineral assemblage in the other sapphirine-free clinopyroxenite is clinopyroxene + garnet + spinel with the clinopyroxene typically showing sieve-textured rims, the garnet completely kelyphitized, and the spinel, as the core of kelyphite, generally rounded and 0.5–1.0 mm in size (Fig. 3e and f).

Table 1
Mineral modal abundance (vol%) and major element data (wt%) of Jiande clinopyroxenite xenoliths.

	Sample	SZZ12-02	SZZ12-09	SZZ12-14
	Rock type	Clinopyroxenite	Clinopyroxenite	Clinopyroxenite
Modes	Cpx[a]	65.0	68.0	79.0
	Grt	22.0	17.0	16.0
	Spl	10.0	11.5	5.00
	Spr	3.00	3.00	0.00
	Pl	0	0.5	0
Major element	SiO_2	39.5	41.1	45.6
	TiO_2	0.10	0.17	0.21
	Al_2O_3	21.6	21.2	13.5
	TFe_2O_3	4.26	4.66	5.96
	MnO	0.07	0.08	0.14
	MgO	15.5	15.5	15.2
	CaO	15.2	14.3	15.9
	Na_2O	0.87	0.90	0.82
	K_2O	0.26	0.20	0.11
	P_2O_5	0.01	0.10	0.20
	Cr_2O_3	0.18	0.22	0.16
	NiO	0.10	0.06	0.03
	LOI	1.92	1.02	1.62
	Total	99.5	99.5	99.4
	Mg#	87.9	86.9	83.6

[a] Grt, garnet; Cpx, clinopyroxene; Spl, spinel; Pl, plagioclase.

3. Analytical method

3.1. Elemental mapping and energy dispersive spectrometry

Elemental mapping and energy dispersive spectrometry were analyzed by SEM on a FEI NOVA nano450 scanning electron microscope at the Institute of Geology and Geophysics (IGG), Chinese Academy of Sciences. They were obtained at 15 kV accelerating voltage and 3.5 nA beam current.

3.2. Major element analysis of whole rocks

Major element analysis was carried out using a Phillips PW 2400 sequential X-ray fluorescence spectrometer (XRF) instrument at the IGG, Chinese Academy of Sciences. The samples were powdered with an agate mill to 200 mesh and 0.5 g powder was mixed with 5 g $Li_2B_4O_7$. A glass bead was formed by fusion.

3.3. Major element analysis of minerals

Major element compositions of minerals were obtained by wavelength-dispersive spectrometry using JEOL JXA8100 electron probe micro analyzer operating at an accelerating voltage of 15 kV, beam current of 10 nA, 5 μm beam spot and 10–30 s counting time on peak. The spot size is 5 μm. The precisions of all analyzed elements are better than 1.5%. The analysis was carried out at the IGG, Chinese Academy of Sciences.

3.4. In-situ trace element analysis of minerals

Trace elements of clinopyroxene were analyzed using a laser ablation inductively coupled plasma mass spectrometer at the State Key Laboratory of Geological Processes and Mineral Resources, China University of Geosciences, Wuhan. The detailed description of the method has been given in Liu et al. (2008). Laser sampling was performed using an ArF excimer laser ablation system (193 nm wavelength), which was connected to an Agilent 7500a ICP-MS instrument with a 1 m transfer tube. A spot size of 60 μm and a repetition rate of 8 Hz were used during the analyses. The NIST SRM 610 glass standard was used as an external calibration standard.

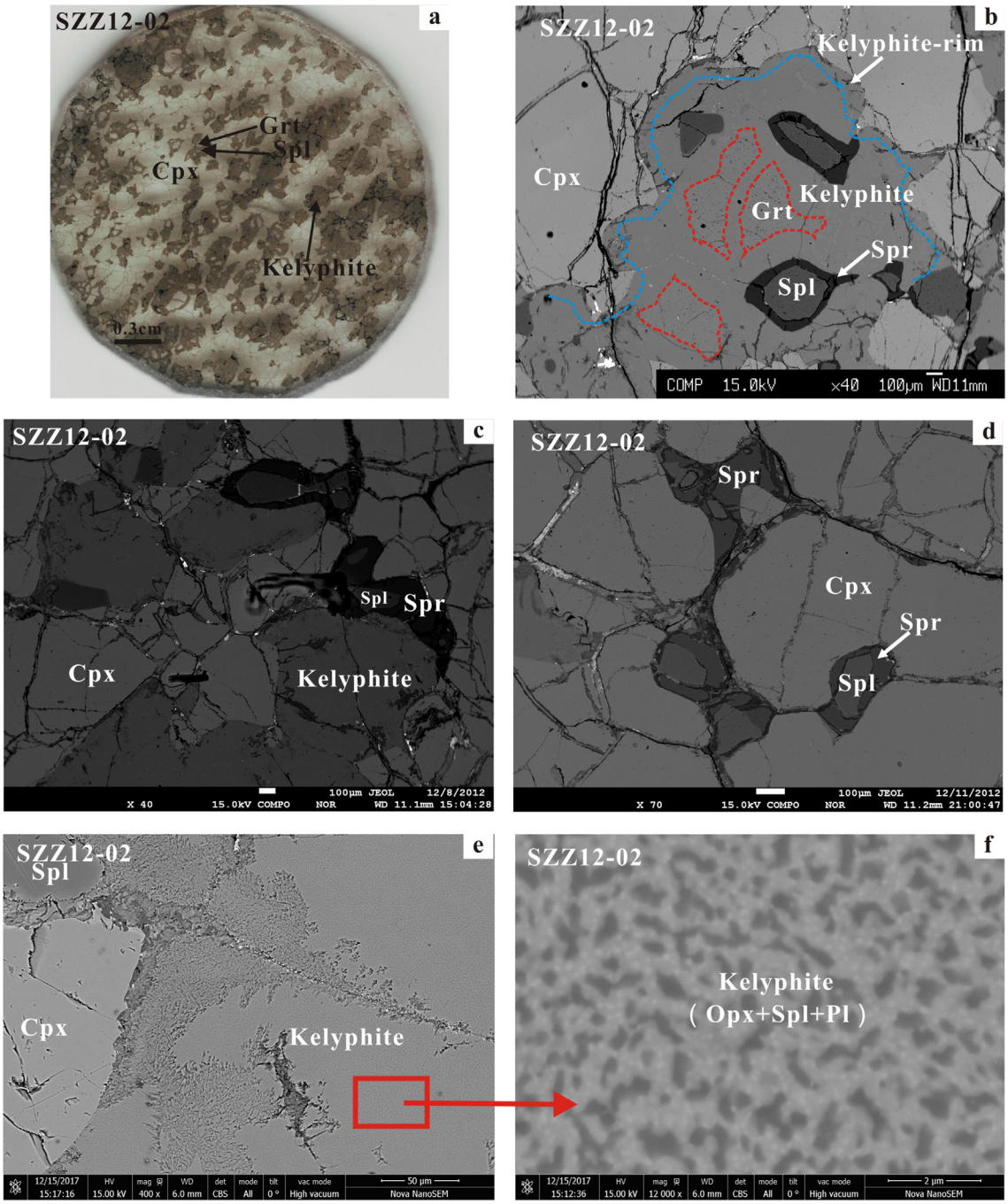

Fig. 2. Photomicrograph of thin section (a) and backscattered electron images of sapphirine (Spr)-bearing clinopyroxenite sample SZZ12-02 (b–f). Garnet (Grt) is partially to completely replaced by kelyphite (b–f). Spinel (Spl) occurs either as inclusions in kelyphite (b) or as discrete grains between adjacent minerals (c, d; clinopyroxene (Cpx) and garnet). Sapphirine (Spr) is anhedral and always surround spinel (b–d). Vermicular intergrowths of plagioclase (dark gray patches), orthopyroxene (light gray background) and spinel (f).

3.5. In-situ lithium (Li) isotopic analysis of clinopyroxene

In-situ Li contents and isotopic compositions of clinopyroxene on thin sections were performed on Cameca IMS-1280 SIMS at IGG, Chinese Academy of Sciences, following the established methods (Su et al., 2015; Zhang et al., 2010). Samples were sputtered with O-primary ion beam at 13 kV and an intensity of about 15 to 30 nA. The spot was approximately 20×30 μm in size. The Li isotopic compositions are expressed as δ^7Li relative to the NIST L-SVEC standard $\{\delta^7\text{Li} = [(^7\text{Li}/^6\text{Li})_{\text{sample}} / (^7\text{Li}/^6\text{Li})_{\text{L-SVEC}} - 1] \times 1000\}$. Clinopyroxene of the peridotite samples 06JY29 and 06JY31 were analyzed multiple times for accuracy check during the course of the analysis and yielded an average δ^7Li value of -2.56 ± 0.70 ($n = 4$) and -2.37 ± 0.48 ($n = 6$), respectively, consistent with the recommended values (Su et al., 2015).

4. Results

Mineral modal abundance and bulk composition of the Jiande clinopyroxenite xenoliths are reported in Table 1. Representative electron microprobe analyses of their minerals are reported in Table 2. Results of in-situ trace element data of clinopyroxene and kelyphite from the Jiande and Hannuoba clinopyroxenite xenoliths are reported in Table 3. In-situ Li isotope analysis of clinopyroxene from Jiande clinopyroxenite xenoliths are reported in Table 4. The temperature

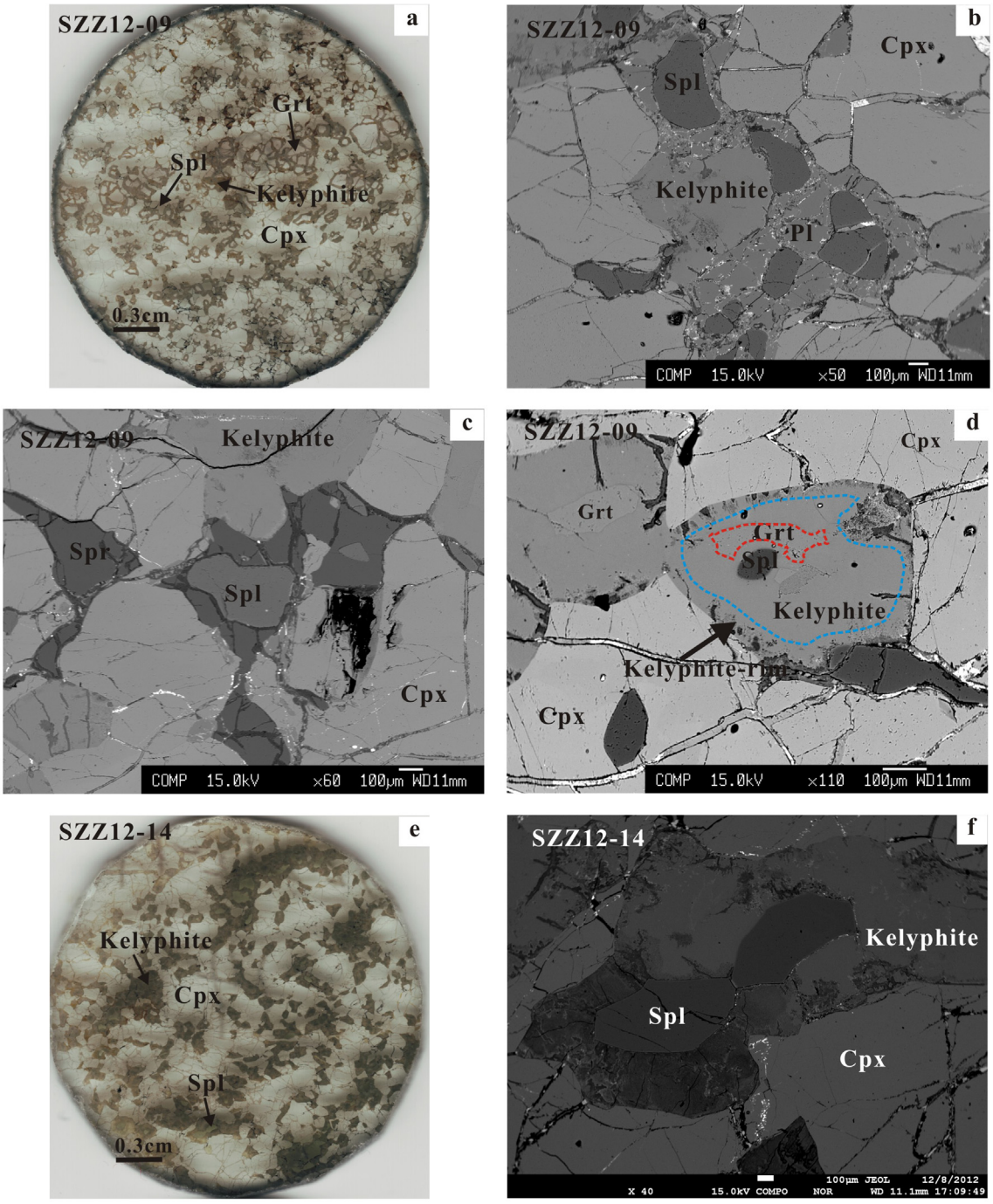

Fig. 3. Photomicrographs of thin section (a, e) and backscattered electron images of sapphirine-bearing clinopyroxenite sample SZZ12-09 and SZZ12-14 (b, c, d and f). Plagioclase (Pl) commonly occurs along the grain boundaries of clinopyroxene and garnet (b). Garnet is partially to completely replaced by kelyphite (b, c, d and f). Spinel occurs either as inclusions in kelyphite or as discrete grains between adjacent minerals (b, c, d and f; clinopyroxene and garnet). Sapphirine is anhedral and surround spinel (c).

and pressure estimates based on different geothermobarometers are provided in Table 5.

4.1. Whole-rock major element composition

The three Jiande clinopyroxenite xenoliths have different bulk chemical compositions (Table 1). The two sapphirine-bearing clinopyroxenite xenoliths are rich in Al_2O_3 (21.2–21.6 wt%) and poor in SiO_2 (39.5–41.1 wt%), similar to the sapphirine-bearing clinopyroxenite xenolith from Hannuoba basalts and sapphirine-bearing garnet pyroxenites from Ronda peridotite massif (Fig. 5; Morishita et al., 2001; Su et al., 2012). The other sapphirine-free clinopyroxenite has lower Al_2O_3 (13.5 wt%), Mg# (83.6) and higher SiO_2 (45.6 wt%) than the two sapphirine-bearing clinopyroxenite samples (Fig. 5 and Table 1).

4.2. Mineral chemistry

4.2.1. Clinopyroxene

Clinopyroxene from the Jiande clinopyroxenite xenoliths has restricted Al_2O_3 (10.5–11.5 wt%), CaO (22.3–22.6 wt%), TiO_2 (0.20–0.27 wt%) contents, and Mg# (89–93) and can be named as aluminous diopside (Morimoto, 1989; Table 2). These clinopyroxenes are similar to those in sapphirine-bearing pyroxenites worldwide and garnet pyroxenites from the Ronda peridotite massif, but different from

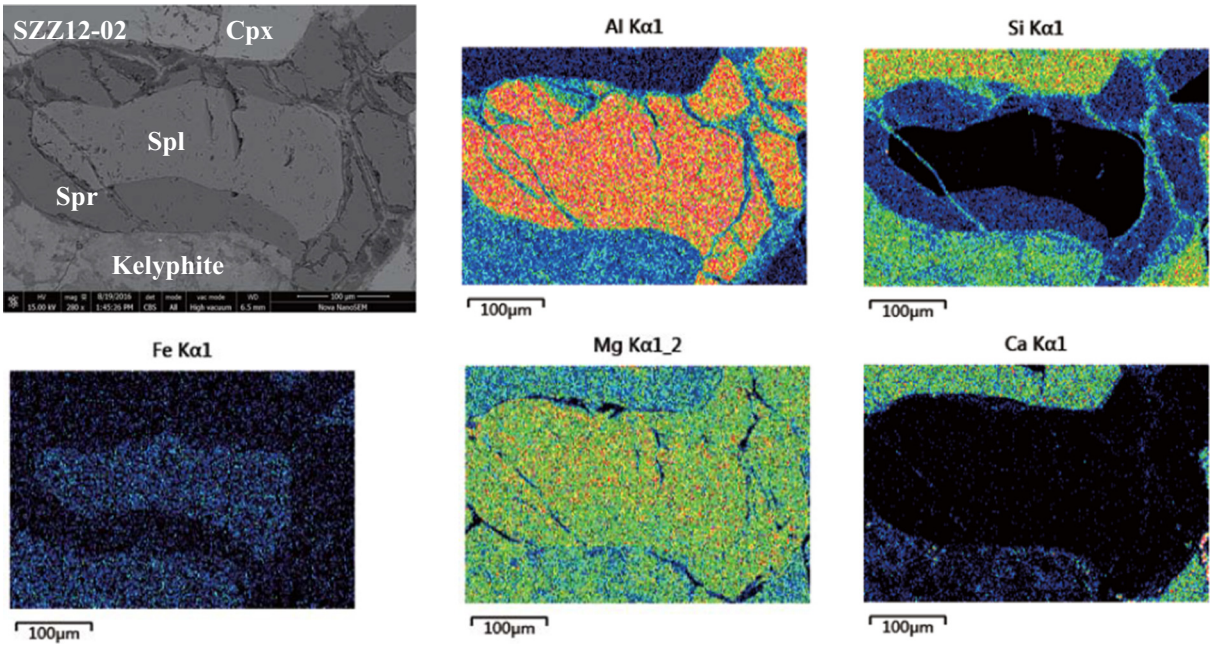

Fig. 4. Backscattered electron images (a) and elemental mapping (b-d) of sapphirine-spinel association.

those in sapphirine-bearing granulites worldwide (Fig. 6a; Arima and Barnett, 1984; Christy, 1989; Gregoire et al., 2001; Griffin and O'Reilly, 1986; Kornprobst et al., 1990; Lal, 1997; Lal et al., 1987; Morishita et al., 2001, 2009; Okay, 1994; Sutherland et al., 2003).

4.2.2. Garnet/kelyphite

Most garnets in these three clinopyroxenite xenoliths are replaced by kelyphites, although rare fresh relic garnets have been observed in the two sapphirine-bearing clinopyroxenite xenoliths (Figs. 2b and 3d). These kelyphites still possess bulk chemical composition almost identical to that of garnets, with only few analyses on the kelyphite rim yielding lower CaO content (Table 2). The garnet/kelyphite is rich in pyrope end-member (pyrope: 62.5–71.4, almandine: 13.4–19.5, grossular: 16.0–18.0) and shows narrow Al_2O_3 (22.7–24.1 wt%), CaO (5.68–8.16 wt%) and TiO_2 (0–0.08 wt%) contents (Table 2). These features are similar to those in garnet pyroxenites from Hannuoba (Hu et al., 2016) and Ronda (Fig. 6b; Morishita et al., 2009). Their CaO and Cr_2O_3 contents mostly fall within the websteritic field (Fig. 6b; Sobolev et al., 1973).

4.2.3. Spinel

Spinel from the Jiande clinopyroxenite xenoliths is magnesian and aluminous (MgO: 20.8–22.9 wt%; Al_2O_3: 64.8–67.9 wt%) with low Cr_2O_3 (0.93–1.99 wt%) and TiO_2 (<0.02 wt%) contents (Table 2). It falls within the field of pyroxenite xenoliths in eastern China (Hu et al., 2016; Su et al., 2012; Xu et al., 1996; Yu et al., 2003), but different from those in sapphirine-bearing granulites and khondalite (Fig. 6c; Arima and Barnett, 1984; Christy, 1989; Griffin and O'Reilly, 1986; Jiao et al., 2015; Lal, 1997; Lal et al., 1987; Santosh et al., 2007; Sutherland et al., 2003).

4.2.4. Sapphirine

Sapphirine from two Jiande clinopyroxenite xenoliths has narrow compositional ranges in SiO_2 (14.5–14.9 wt%), Al_2O_3 (60.9–61.7 wt%), MgO (19.7–20.1 wt%), FeO (2.41–2.73 wt%) and Cr_2O_3 (0.44–0.96 wt%) (Table 2). It has a general formula of $(Mg_{3.48}Fe_{0.26}Ni_{0.01})^{IV}(Al_{8.48}Cr_{0.05})^{VI}Si_{1.72}O_{20}$ (Table 2), which shows higher MgO and Cr_2O_3 than those from pyroxenites, granulites and khondalite worldwide (Fig. 6d; Arima and Barnett, 1984; Christy, 1989; Gregoire et al., 2001; Griffin and O'Reilly, 1986; Jiao et al., 2015; Kornprobst et al., 1990; Lal, 1997; Lal et al., 1987; Morishita et al., 2001; Okay, 1994; Santosh et al., 2007; Su et al., 2012; Sutherland et al., 2003).

4.3. Trace element compositions of clinopyroxene and kelyphite

Clinopyroxene is homogeneous within and between grains in the Jiande clinopyroxenite xenoliths and displays a convex-upward REE pattern (Fig. 7a). The depletion of HREE in clinopyroxene may be due to partitioning into co-existing garnet. However, clinopyroxene from the Hannuoba sapphirine-bearing clinopyroxenite xenolith displays an almost flat REE pattern (Fig. 7a). Notably, their trace element patterns are similar, showing negative anomalies of the HFSE (i.e., Zr, Nb, Y and Ti; Fig. 7b). Different from garnet pyroxenites from the Ronda, sapphirine-bearing clinopyroxenite xenoliths from Jiande and Hannuoba do not show positive Eu-Sr anomalies (Fig. 6a, b; Morishita et al., 2009).

Kelyphite in the Jiande clinopyroxenite xenoliths is characterized by LREE-depleted pattern (Fig. 7c). In primitive mantle-normalized trace element diagrams, it has a remarkable positive U anomaly and negative Ti and Y anomalies without positive Eu and negative Sr anomalies (Fig. 7d).

4.4. The Li isotopic composition of clinopyroxene

Clinopyroxene in the Jiande clinopyroxenite xenoliths shows homogeneous Li abundances (1.04–1.63 ppm), much lower than those in garnet pyroxenites from Hannuoba (1.61–79.8 ppm) and Ronda (10–20 ppm), and crustal ecolgites (>8.6 ppm) (Fig. 8a, b and Table 4; Morishita et al., 2009; Su et al., 2014; Woodland et al., 2002). The δ^7Li value (−3.31 to −12.19‰) of clinopyroxene is also lower than that of the normal mantle (2–6‰; Tomascak et al., 2008) and those in Hannuoba pyroxenites (−5.7–13.2‰; Fig. 8b and Table 4; Su et al., 2014).

4.5. Temperature and pressure estimates

Equilibrium partitioning of Mg-Fe between clinopyroxene and kelyphite, as indicated by the 1:1 linear correlations between the Mg# of these two minerals (not shown), permits temperature estimates for the Jiande clinopyroxenite xenoliths. Temperatures estimated using three different garnet-clinopyroxene Fe-Mg thermometers fall within

Table 2
Representative chemical composition of minerals in Jiande clinopyroxenite xenoliths (wt%).

Sample	SZZ12-02																	SZZ12-02				SZZ1209					
Mineral	Cpx1[a]	Cpx2	Cpx3	Grt1	Grt2	Grt3	Kelyphite1			Kelyphite2	Kelyphite3	Spl1	Spr1	Spl2	Spr2	Spl3	Spr3	Spl4	Spr4	Spl5	Spr5	Cpx1	Cpx2	Cpx3	Grt1	Grt2	Grt3
							Core	Mantle	Rim			in Grt	beside cpx	Core	Spr rim	Core	Spr rim	Core	Spr rim	Core	Spr rim						
SiO_2	49.3	49.5	49.1	43.0	42.7	42.9	43.3	42.6	42.7	43.3	42.1	0.00	14.8	0.00	14.7	0.00	14.5	0.00	14.6	0.00	14.5	48.9	49.9	49.1	42.5	42.7	42.4
TiO_2	0.08	0.10	0.11	0.04	0.01	0.04	0.04	0.03	0.08	0.04	0.01	0.01	0.04	0.02	0.04	0.00	0.00	0.01	0.01	0.01	0.00	0.11	0.14	0.13	0.00	0.06	0.01
Al_2O_3	11.4	11.3	11.5	23.5	23.8	23.2	23.9	24.1	23.7	23.9	23.9	66.6	61.3	66.2	61.7	66.4	61.4	66.5	60.9	67.1	61.7	12.3	10.8	11.6	23.7	23.7	23.3
Cr_2O_3	0.26	0.31	0.23	0.17	0.20	0.20	0.15	0.18	0.18	0.15	0.18	1.87	0.96	1.99	0.70	1.35	0.86	1.56	0.68	1.52	0.70	0.26	0.26	0.26	0.18	0.18	0.15
FeO	1.99	1.86	1.92	7.11	7.10	6.87	6.77	6.90	6.94	6.77	6.86	7.06	2.55	7.12	2.48	7.17	2.41	7.20	2.56	7.18	2.57	2.16	1.88	1.84	7.36	7.42	7.48
MnO	0.04	0.03	0.06	0.22	0.21	0.21	0.18	0.20	0.20	0.18	0.18	0.02	0.03	0.03	0.01	0.01	0.00	0.05	0.00	0.02	0.05	0.06	0.06	0.00	0.22	0.28	0.26
MgO	13.7	13.8	13.7	20.5	20.5	20.5	20.0	20.1	20.7	20.0	19.9	22.8	20.0	22.8	19.8	22.8	19.9	22.9	19.8	22.5	20.1	13.2	13.7	13.3	20.0	20.1	19.8
CaO	22.3	22.2	22.2	6.32	6.35	6.44	6.31	6.30	5.82	6.31	6.16	0.00	0.06	0.00	0.05	0.00	0.09	0.00	0.04	0.00	0.07	22.2	22.7	22.7	6.35	6.54	6.54
Na_2O	1.09	1.01	1.06	0.00	0.00	0.00	0.00	0.00	0.01	0.00	0.00	0.00	0.02	0.00	0.00	0.00	0.01	0.00	0.00	0.00	0.01	1.01	1.04	0.97	0.01	0.00	0.01
K2O	0.00	0.00	0.00	0.00	0.00	0.00	0.00	0.00	0.00	0.00	0.00	0.00	0.00	0.00	0.00	0.00	0.00	0.00	0.00	0.00	0.00	0.00	0.00	0.00	0.00	0.00	0.00
NiO	0.03	0.03	0.05	0.00	0.02	0.02	0.00	0.00	0.01	0.00	0.01	0.38	0.15	0.41	0.14	0.38	0.14	0.36	0.15	0.34	0.12	0.01	0.01	0.05	0.00	0.00	0.00
Total	100	100	99.9	101	101	100	101	100	100	101	99.2	98.7	99.9	98.6	99.6	98.1	99.3	98.6	98.8	98.7	99.8	100	100	100.0	100	101	99.9
Mg#	92.5	93.0	92.8	83.8	83.9	84.3	84.2	84.0	84.3	84.2	83.9	85.3	93.4	85.2	93.5	85.1	93.7	85.1	93.3	84.9	93.4	91.7	92.9	92.9	83.0	82.9	82.6
O=	6	6	6	12	12	12	12	12	12	12	12	4	20	4	20	4	20	4	20	4	20	6	6	6	12	12	12
Si	1.777	1.784	1.777	3.013	2.991	3.018	3.032	2.995	3.001	3.033	2.994	0.000	1.727	0.000	1.718	0.000	1.702	0.000	1.721	0.000	1.699	1.764	1.795	1.776	2.997	2.997	3.007
Ti	0.002	0.003	0.003	0.002	0.001	0.002	0.002	0.002	0.004	0.002	0.001	0.000	0.003	0.000	0.004	0.000	0.000	0.000	0.001	0.000	0.000	0.003	0.004	0.004	0.000	0.003	0.001
Al	0.486	0.479	0.489	1.941	1.967	1.924	1.969	1.997	1.965	1.969	2.000	1.960	8.432	1.953	8.497	1.963	8.495	1.958	8.471	1.975	8.489	0.525	0.460	0.493	1.973	1.961	1.948
Cr	0.007	0.009	0.007	0.010	0.011	0.011	0.008	0.010	0.010	0.008	0.010	0.037	0.089	0.039	0.064	0.027	0.079	0.031	0.064	0.030	0.065	0.008	0.008	0.007	0.010	0.010	0.009
Fe^{2+}	0.060	0.056	0.058	0.416	0.416	0.405	0.396	0.405	0.408	0.396	0.408	0.144	0.249	0.141	0.242	0.140	0.237	0.140	0.252	0.150	0.251	0.065	0.057	0.056	0.434	0.436	0.444
Fe^{3+}												0.003		0.008		0.010		0.011		0.000								
Mn	0.001	0.001	0.002	0.013	0.013	0.012	0.011	0.012	0.012	0.011	0.011	0.000	0.002	0.001	0.001	0.000	0.000	0.001	0.001	0.000	0.004	0.002	0.002	0.000	0.013	0.017	0.016
Mg	0.739	0.743	0.737	2.140	2.144	2.154	2.086	2.107	2.170	2.084	2.107	0.848	3.484	0.852	3.453	0.852	3.472	0.852	3.481	0.837	3.495	0.708	0.734	0.719	2.104	2.099	2.091
Ca	0.862	0.860	0.860	0.474	0.477	0.486	0.473	0.474	0.438	0.473	0.469	0.000	0.008	0.000	0.006	0.000	0.011	0.000	0.006	0.000	0.008	0.858	0.873	0.881	0.480	0.492	0.497
Na	0.076	0.071	0.075	0.000	0.000	0.000	0.000	0.000	0.001	0.000	0.000	0.000	0.004	0.000	0.000	0.000	0.001	0.000	0.000	0.000	0.002	0.071	0.072	0.068	0.001	0.000	0.002
K	0.000	0.000	0.000	0.000	0.000	0.000	0.000	0.000	0.000	0.000	0.000	0.000	0.000	0.000	0.000	0.000	0.000	0.000	0.000	0.000	0.000	0.000	0.000	0.000	0.000	0.000	0.000
Ni	0.001	0.001	0.001	0.000	0.001	0.001	0.000	0.000	0.000	0.000	0.000	0.008	0.014	0.008	0.013	0.008	0.013	0.007	0.014	0.007	0.011	0.000	0.000	0.001	0.000	0.000	0.000
Total	4.012	4.004	4.008	8.009	8.018	8.012	7.977	8.001	8.008	7.976	8.000	3.000	13.998	2.995	13.985	2.997	13.998	3.000	13.996	2.991	14.025	4.003	4.003	4.003	8.012	8.014	8.014

(continued on next page)

Table 2 (*continued*)

Sample	SZZ12-09							SZZ12-09						SZZ12-14									
Mineral	Kelyphite1		Kelyphite2	Kelyphite3	Spl1	Spl2	Spr2	Spl3	Spr3	Spr4	Pl1	Pl2	Pl3	Cpx1	Cpx2	Cpx3	Kelyphite1			Kelyphite2	Kelyphite3	Spl1	Spl2	Spl3
	Core	Rim			in Grt	Core	Spr rim	Core	Spr rim		An-rich	An-rich	An-rich				Core	Mantle	rim			in Grt	in Grt	in Grt
SiO_2	42.5	42.5	42.4	42.5	0.00	0.00	14.5	0.00	14.5	14.9	47.3	47.3	47.4	48.7	49.0	49.1	42.1	42.3	41.8	42.6	41.9	0.00	0.00	0.00
TiO_2	0.05	0.03	0.04	0.00	0.00	0.00	0.03	0.01	0.01	0.00	0.01	0.00	0.00	0.17	0.18	0.17	0.03	0.02	0.06	0.00	0.02	0.00	0.04	0.02
Al_2O_3	24.0	23.8	24.0	24.1	66.9	67.2	60.6	67.9	61.7	61.8	33.5	33.8	33.4	11.5	10.4	11.5	23.5	24.1	22.7	23.6	23.4	64.8	65.3	65.6
Cr_2O_3	0.11	0.18	0.16	0.12	1.53	0.93	0.48	0.94	0.44	0.49	0.03	0.00	0.00	0.17	0.20	0.20	0.17	0.15	0.20	0.15	0.17	1.68	1.69	1.67
FeO	7.31	7.15	7.16	7.11	7.33	7.61	2.73	7.61	2.71	2.70	0.12	0.05	0.07	2.90	2.79	3.15	9.29	8.60	10.17	8.97	9.37	10.2	10.3	10.4
MnO	0.24	0.26	0.22	0.28	0.04	0.05	0.04	0.05	0.04	0.05	0.02	0.05	0.00	0.08	0.07	0.06	0.32	0.26	0.38	0.29	0.33	0.08	0.05	0.07
MgO	19.6	19.2	19.7	19.9	22.9	22.5	19.7	22.3	19.7	19.9	0.02	0.04	0.04	13.3	13.3	13.3	17.5	16.1	19.5	16.8	17.7	20.9	20.9	20.8
CaO	6.41	6.73	6.47	6.53	0.00	0.00	0.07	0.00	0.08	0.12	17.0	17.0	16.8	21.8	22.4	21.7	7.01	8.16	5.68	7.64	6.74	0.00	0.00	0.00
Na_2O	0.00	0.00	0.00	0.00	0.00	0.00	0.02	0.00	0.01	0.02	1.98	1.92	1.98	1.06	0.98	1.08	0.00	0.00	0.00	0.00	0.00	0.00	0.00	0.00
K2O	0.00	0.00	0.00	0.00	0.00	0.00	0.00	0.00	0.00	0.00	0.00	0.00	0.00	0.00	0.00	0.00	0.00	0.00	0.00	0.00	0.00	0.00	0.00	0.00
NiO	0.01	0.01	0.01	0.00	0.33	0.33	0.12	0.34	0.13	0.12	0.00	0.00	0.02	0.01	0.00	0.00	0.00	0.01	0.00	0.00	0.00	0.31	0.32	0.35
Total	100	99.8	100	101	99.0	98.6	98.3	99.2	99.2	100	100	100	99.7	99.7	99.3	100.1	100.0	99.7	100.4	100.1	99.6	98.0	98.6	98.9
Mg#	82.8	82.8	83.2	83.4	84.9	84.2	92.9	84.1	92.9	93.0	27.3	58.9	53.4	89.2	89.6	88.3	77.3	77.1	77.5	77.1	77.3	78.6	78.5	78.2
O=	12	12	12	12	4	4	20	4	20	20	8	8	8	6	6	6	12	12	12	12	12	4	4	4
Si	2.998	3.015	2.995	2.992	0.000	0.000	1.722	0.000	1.698	1.730	2.172	2.167	2.181	1.771	1.792	1.777	3.011	3.029	2.985	3.043	3.007	0.000	0.000	0.000
Ti	0.003	0.001	0.002	0.000	0.000	0.000	0.002	0.000	0.001	0.000	0.000	0.000	0.000	0.005	0.005	0.005	0.002	0.001	0.003	0.000	0.001	0.000	0.001	0.000
Al	1.996	1.985	1.995	1.998	1.964	1.978	8.465	1.986	8.533	8.480	1.815	1.826	1.811	0.492	0.449	0.491	1.984	2.036	1.912	1.986	1.984	1.952	1.955	1.958
Cr	0.006	0.010	0.009	0.007	0.030	0.018	0.045	0.018	0.041	0.045	0.001	0.000	0.000	0.005	0.006	0.006	0.010	0.008	0.012	0.009	0.010	0.034	0.034	0.033
Fe^{2+}	0.432	0.424	0.423	0.418	0.144	0.155	0.271	0.158	0.266	0.263	0.004	0.002	0.003	0.088	0.085	0.095	0.556	0.515	0.608	0.536	0.563	0.198	0.204	0.208
Fe^{3+}					0.009	0.004		0.000														0.019	0.014	0.011
Mn	0.014	0.015	0.013	0.016	0.001	0.001	0.004	0.001	0.004	0.005	0.001	0.002	0.000	0.003	0.002	0.002	0.020	0.016	0.023	0.018	0.020	0.002	0.001	0.001
Mg	2.063	2.025	2.073	2.082	0.849	0.839	3.490	0.826	3.446	3.457	0.002	0.003	0.003	0.723	0.723	0.715	1.870	1.714	2.072	1.785	1.892	0.795	0.790	0.783
Ca	0.485	0.511	0.490	0.492	0.000	0.000	0.009	0.000	0.010	0.014	0.836	0.834	0.828	0.851	0.878	0.841	0.538	0.626	0.435	0.584	0.518	0.000	0.000	0.000
Na	0.000	0.000	0.000	0.000	0.000	0.000	0.004	0.000	0.003	0.004	0.176	0.171	0.177	0.075	0.070	0.076	0.000	0.000	0.000	0.000	0.001	0.000	0.000	0.000
K	0.000	0.000	0.000	0.000	0.000	0.000	0.000	0.000	0.000	0.000	0.000	0.000	0.000	0.000	0.000	0.000	0.000	0.000	0.000	0.000	0.000	0.000	0.000	0.000
Ni	0.000	0.001	0.000	0.000	0.007	0.007	0.011	0.007	0.012	0.012	0.000	0.000	0.001	0.000	0.000	0.000	0.000	0.000	0.000	0.000	0.000	0.006	0.006	0.007
Total	7.997	7.986	8.001	8.006	3.003	2.995	14.012	2.991	14.003	14.010	5.007	5.005	5.001	4.013	4.010	4.008	7.990	7.947	8.050	7.960	7.996	3.000	2.999	3.003

Table 3
Mineral trace element compositions of Jiande clinopyroxenite xenoliths (in ppm).

Sample	SZZ12-02		SSZ12-09		SZZ12-14		JSB10-57[a]
Mineral	Kelyphite	Cpx	Kelyphite	Cpx	Cpx	Kelyphite	Cpx
Li	5.21	1.50	2.42	1.11	1.34	0.11	7.96
P	12.9	6.90	12.3	7.20	45.1	48.5	32.2
Sc	60.1	7.59	109	11.4	21.9	111	47.0
Ti	147	742	115	549	815	155	712
V	53.0	226	44.9	148	285	70.0	250
Cr	1734	2121	1230	911	967	839	683
Mn	2013	247	2165	307	521	2578	717
Co	62.8	21.7	53.8	18.1	34.1	66.4	17.1
Ni	29.8	237	23.6	194	236	25.4	134
Cu	10.0	1.56	1.14	1.50	1.53	0.20	2.10
Zn	4.50	3.04	3.96	2.35	11.0	10.9	0.76
Ga	3.00	7.70	6.43	4.61	11.5	3.33	4.15
Ge	1.84	1.00	2.95	1.25	1.22	1.59	1.00
Rb	0.34	0.37	0.21	0.12	0.05	0.05	0.05
Sr	3.89	3.23	2.73	1.96	1.37	0.01	25.5
Y	11.4	0.53	16.2	0.74	1.68	13.0	5.64
Zr	1.64	0.74	2.14	0.61	0.46	0.91	1.26
Nb	0.08	0.05	0.08	0.05	0.01	0.02	0.09
Mo	0.31	0.27	0.43	0.29	0.01	0.01	0.03
Cs	0.26	0.20	0.28	0.10	0.02	0.03	0.02
Ba	2.59	0.71	1.37	0.30	0.07	0.01	0.03
La	0.11	0.06	0.12	0.07	0.01	0.01	0.62
Ce	0.13	0.07	0.12	0.07	0.01	0.01	1.50
Pr	0.07	0.03	0.06	0.03	0.01	0.01	0.15
Nd	0.31	0.24	0.31	0.22	0.21	0.05	0.68
Sm	0.33	0.23	0.24	0.22	0.17	0.14	0.28
Eu	0.17	0.12	0.16	0.13	0.09	0.13	0.12
Gd	0.92	0.52	0.95	0.55	0.39	0.61	0.57
Tb	0.20	0.07	0.23	0.07	0.07	0.18	0.13
Dy	1.69	0.18	2.24	0.23	0.45	1.72	1.05
Ho	0.44	0.03	0.56	0.03	0.08	0.49	0.22
Er	1.33	0.08	1.79	0.07	0.17	1.70	0.62
Tm	0.19	0.02	0.33	0.02	0.02	0.26	0.10
Yb	1.14	0.10	2.17	0.12	0.11	1.93	0.65
Lu	0.16	0.04	0.33	0.04	0.01	0.30	0.07
Hf	0.19	0.11	0.20	0.12	0.05	0.05	0.08
Ta	0.05	0.02	0.03	0.02	0.01	0.01	0.01
W	0.22	0.10	0.23	0.12	0.01	0.01	0.02
Pb	0.08	0.05	0.06	0.05	0.01	0.03	0.08
Th	0.03	0.01	0.02	0.01	0.01	0.01	0.01
U	0.03	0.01	0.03	0.01	0.01	0.01	0.01
$(La/Yb)_N$	0.06	0.41	0.04	0.37	0.06	0.01	0.64

[a] Hannuoba clinopyroxene from Su et al. (2012).

Table 4
Li concentration and isotopic composition of clinopyroxene in Jiande clinopyroxenite xenoliths and reference materials.

Sample	Mineral	Position	Spot	δ^7Li	1se	Li ppm	1se
SZZ12-02	Cpx1	Rim	1	−7.15	0.67	1.32	0.01
Clinopyroxenite		Core	2	−7.43	0.57	1.48	0.01
(Cpx + Grt + Spl + Spr)	Cpx2	Rim	1	−5.43	0.60	1.32	0.01
		Mantle	2	−7.11	0.66	1.34	0.01
		Core	3	−7.68	0.57	1.48	0.01
	Cpx3	Rim	1	−3.31	0.56	1.17	0.01
		Core	2	−6.20	0.56	1.45	0.01
		Average		−6.33		1.37	
SZZ12-09	Cpx1	Rim	1	−6.72	0.57	1.17	0.01
Clinopyroxenite		Core	2	−7.33	0.61	1.49	0.01
(Cpx + Grt + Spl + Spr)	Cpx2	Rim	1	−4.07	0.79	1.04	0.01
		Core	2	−5.55	0.63	1.27	0.01
	Cpx3	Rim	1	−6.58	0.53	1.27	0.01
		Core	2	−6.94	0.69	1.25	0.01
		Average		−6.20		1.25	
SZZ12-14	Cpx1	Rim	1	−11.16	0.58	1.26	0.01
Clinopyroxenite		Core	2	−10.44	0.57	1.63	0.02
(Cpx + Grt + Spl)	Cpx2	Rim	1	−10.27	0.64	1.30	0.01
		Core	2	−12.19	0.53	1.23	0.01
	Cpx3	Rim	1	−10.03	0.67	1.29	0.01
		Core	2	−9.56	0.73	1.20	0.01
	Cpx4	Rim	1	−10.36	0.65	1.07	0.01
		Core	2	−10.61	0.65	1.29	0.01
		Average		−10.58		1.28	
Standard							
06JY29	Cpx		1	−2.21	0.76		
Peridotite xenolith			2	−2.93	0.79		
			3	−2.31	0.68		
			4	−2.80	0.70		
06JY31	Cpx		1	−2.46	0.70		
Peridotite xenolith			2	−1.61	0.65		
			3	−2.82	0.64		
			4	−2.40	0.58		
			5	−2.88	0.72		
			6	−2.04	0.74		

the ranges of 967–1138 °C, with an agreement well within 50 °C (Table 5; Dahl, 1980; Krogh, 1988; Powell, 1985). Temperatures estimated from sapphirine-spinel Fe^{2+}-Mg exchange thermometer vary from 1069 to 1094 at a pressure of 8–10 kbar (Table 5; Sato et al., 2006; Su et al., 2012).

5. Discussion

Abundant garnet-bearing pyroxenites are also found in the Hannuoba Cenozoic basalts in the northern margin of the North China Craton and the Ronda peridotite massif, southern Spain (Hu et al., 2016; Liu et al., 2005; Morishita et al., 2001, 2003, 2009; Su et al., 2012). The garnet pyroxenite xenoliths in Hannuoba basalts were considered to have been produced by interaction between peridotite and melt, which resulted in formation of pyroxene and garnet at the expense of olivine (Liu et al., 2005). By contrast, Morishita et al. (2001, 2003, 2009) suggested a gabbro protolith origin for the garnet pyroxenites from Ronda.

Below, we first focus on the origin of sapphirine and garnet/kelyphite and the reactions in their formation. Subsequently, we discuss the protolith of the Jiande clinopyroxenite xenoliths compared with garnet pyroxenite in the Hannuoba basalts and Ronda peridotite massif and reconstruct their P-T path.

5.1. Origin of sapphirine in Jiande clinopyroxenite xenolith

Crustal-derived and mantle-derived sapphirine-bearing rocks usually display distinct chemical composition in their minerals (Fig. 6; Su et al., 2012). The sapphirine in two Jiande clinopyroxenite xenoliths has low Al_2O_3, high MgO and coexists with high Mg# minerals (clinopyroxene, spinel). These characteristics are similar to those in sapphirine-bearing mantle-derived pyroxenites reported in the literatures (Fig. 6d; Griffin and O'Reilly, 1986; Su et al., 2012). Previous studies revealed that the occurrence of mantle-derived sapphirine is restricted to rocks rich in Ca, Al and Mg, where the stable assemblage is aluminous clinopyroxene + garnet + plagioclase + sapphirine (±orthopyroxene ± hornblende) or aluminous clinopyroxene + spinel + sapphirine (±orthopyroxene) (Bilal, 2016; Griffin and O'Reilly, 1986; Kornprobst et al., 1990; Morishita et al., 2001; Su et al., 2012). On the contrary, the mineral assemblage of the Jiande clinopyroxenite xenolith (clinopyroxene + spinel + garnet/kelyphite

Table 5
Temperature (°C) estimates for Jiande clinopyroxenite xenoliths.

Sample	Rock type	T (°C)			
		T(80D)[a]	T(85P)[b]	T(88 K)[c]	T(2006S)[d]
SZZ12-02	Clinopyroxenite	1013	1040	1019	1069–1094
SZZ12–09	Clinopyroxenite	967	1019	997	1072–1090
SZZ12–14	Clinopyroxenite	1138	1059	1055	

[a] Dahl (1980) Cpx-Grt thermometer;
[b] Powell (1985) Cpx-Grt thermometer;
[c] Krogh (1988) Cpx-Grt thermometer;
[d] Sato et al. (2006) Spr-Spl thermometer;

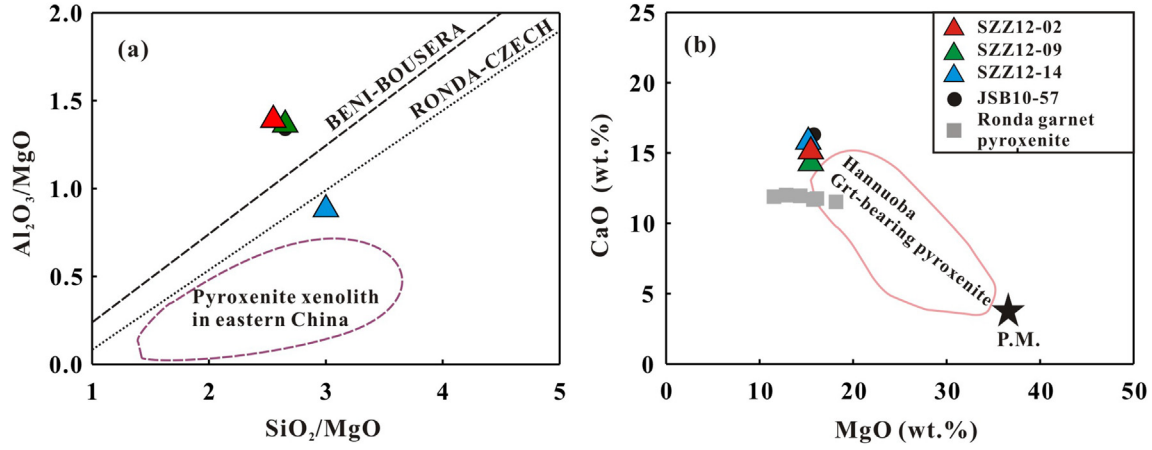

Fig. 5. Al_2O_3/MgO versus SiO_2/MgO (a) and MgO versus CaO (b) for Jiande clinopyroxenite xenoliths. Mantle-derived cumulative pyroxenites from eastern China (purple field) are shown for comparison. The data of sapphirine-bearing clinopyroxenite JSB10-57 in the Hannuoba are from Su et al. (2012). Black dashed lines represent compositional trends for pyroxenites from Beni-Bousera and eclogite-garnet pyroxenites from Ronda and Czech Republic, respectively (Kornprobst et al., 1990; Morishita et al., 2001; Obata et al., 2006). The star denotes the composition of primitive mantle (P.M.) from McDonough and Sun (1995). (For interpretation of the references to colour in this figure legend, the reader is referred to the web version of this article.)

+ sapphirine) is not stable. Sapphirine in this study displays different stages of spinel replacement, from thin rim on the spinel (Figs. 2b, e, f and 3c) to resorbed spinel relics inside newly formed sapphirine (Figs. 2c, d and 3c). Thus, sapphirine in this study is considered to be of metamorphic origin. In addition, the sapphirine-spinel associations can occur either inside the garnet or at the contact between

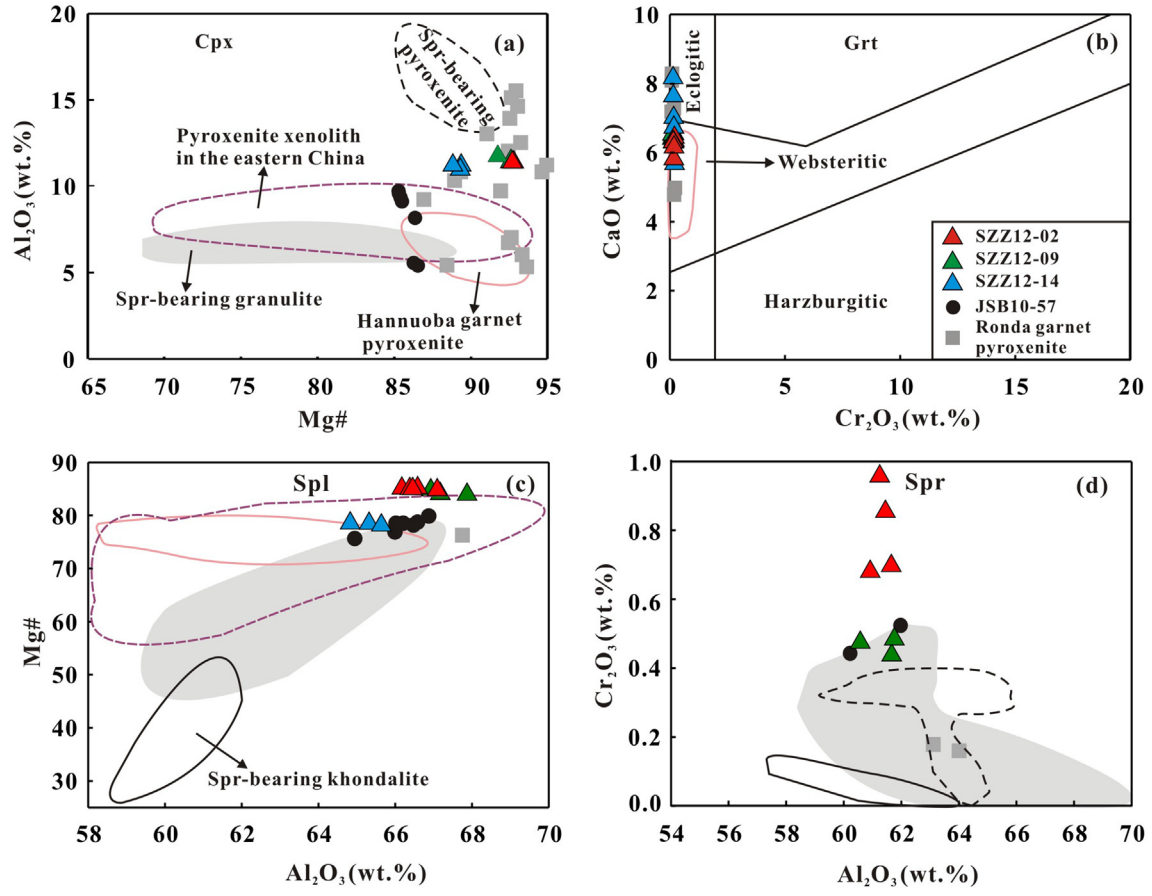

Fig. 6. The chemical compositions of clinopyroxene (a), garnet (b), spinel (c) and sapphirine (d) in the studied samples. The compositions of clinopyroxene, garnet, spinel and sapphirine from different settings, including khondalite (black solid line), granulite (gray field), and pyroxenite (black dash line) are plotted for comparison (Arima and Barnett, 1984; Christy, 1989; Gregoire et al., 2001; Griffin and O'Reilly, 1986; Jiao et al., 2015; Kornprobst et al., 1990; Lal, 1997; Lal et al., 1987; Okay, 1994; Santosh et al., 2007; Sutherland et al., 2003). The pink solid line represents the compositional field for Hannuoba garnet pyroxenite (Hu et al., 2016). The purple dashed line represents the compositional field for pyroxenite cumulate xenolith in the eastern China (Huang et al., 2004; Xu et al., 1996; Yu et al., 1998, 2003). The data of garnet pyroxenites in Ronda peridotite massif, Spain are from Morishita et al. (2001, 2009). The fields for eclogitic, websteritic, and harzburgitic garnets in the Fig. 6b are from Sobolev et al. (1973). (For interpretation of the references to colour in this figure legend, the reader is referred to the web version of this article.)

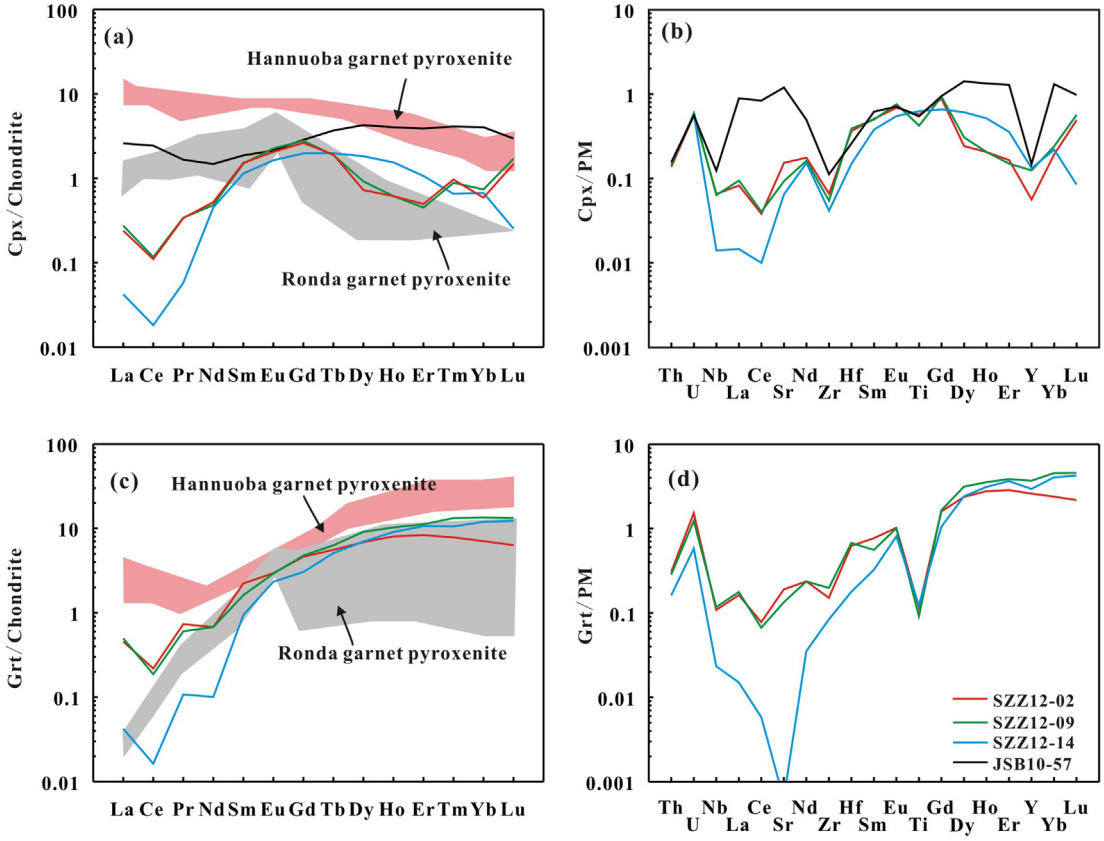

Fig. 7. Chondrite-normalized REE patterns and primitive mantle-normalized trace element spider diagrams for the clinopyroxene (a, b) and garnet (c, d) in the studied samples. Chondrite and primitive mantle (PM) values are from Anders and Grevesse (1989) and McDonough and Sun (1995), respectively. Gray and pink fields in the Fig. 7a and c represent clinopyroxene and garnet trace element data of garnet pyroxenites in the Ronda peridotite massif, Spain and Hannuoba basalts, China, respectively (Morishita et al., 2009; Zhao et al., 2017). (For interpretation of the references to colour in this figure legend, the reader is referred to the web version of this article.)

clinopyroxene and garnet. These indicate that spinel and garnet ought to be the reactants. The subsolidus reaction involved in the formation of aluminous sapphirine is represented as follows: spinel + garnet = sapphirine + clinopyroxene + orthopyroxene. Since the clinopyroxene-sapphirine stability is defined by garnet-consuming reactions (Christy, 1989), sapphirine grows at the expense of spinel during the cooling/uplift process, whilst the Ca-rich garnet is consumed.

5.2. Origin of garnet and the sequence of kelyphitization process in the Jiande clinopyroxenite xenolith

The kelyphite typically forms large grains and usually includes relics of garnet and spinel, similar to the garnet pyroxenite xenoliths from Hannuoba (Figs. 2 and 3; Hu et al., 2016; Liu et al., 2005). Most kelyphites in this study have similar chemical composition to relic garnets. This

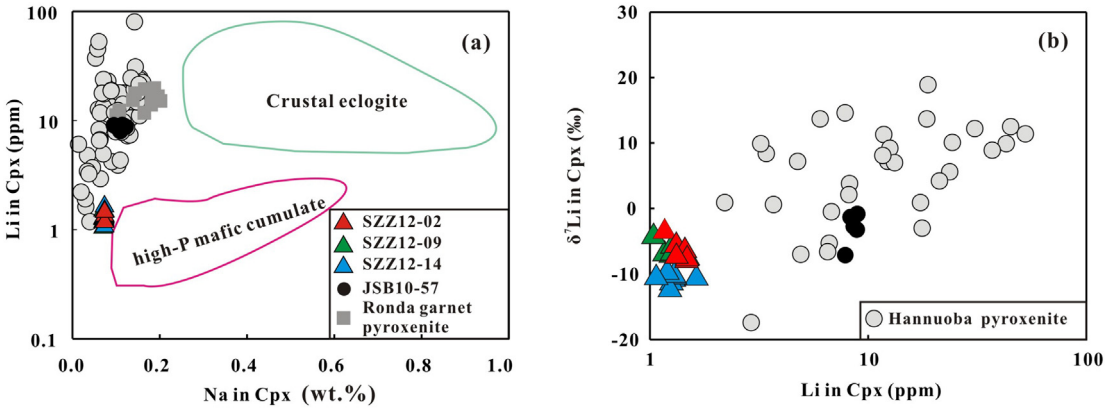

Fig. 8. Li content vs. Li isotope of individual spot analyses in clinopyroxene from studied samples compared to those in pyroxenites from Hannuoba basalts and Ronda peridotite massif (a). Relationship between Li content and Na content of clinopyroxene (b). The data of sapphirine-bearing clinopyroxenite JSB10-57 in the Hannuoba are from Su et al. (2014). The Li content and Li isotopic composition of clinopyroxene in the Hannuoba pyroxenites (a) and Ronda garnet pyroxenites (b) are from Su et al. (2014) and Morishita et al. (2009), respectively. The field for crustal eclogite and high-P mafic cumulate in the Fig. 8a are from Woodland et al. (2002).

feature demonstrates that upon further ascent and decompression, garnet eventually became unstable, starting to break down according to the following reaction: garnet = orthopyroxene + spinel + plagioclase (Obata et al., 2013). Thereafter, the isochemical kelyphite was formed essentially in a chemically-closed system (Naemura et al., 2009; Obata et al., 2013). In addition, the relic spinel displays embayed and round grain boundaries, suggesting that garnet was formed at a later stage at the expense of spinel. Specifically, the Jiande clinopyroxenite xenoliths have different mineral compositions from the Hannuoba garnet pyroxenite (Figs. 5 and 6a-c; Hu et al., 2016). Furthermore, the clinopyroxene and kelyphite from the Jiande clinopyroxenite xenoliths have much lower REE contents than those in Hannuoba (Fig. 6a; Zhao et al., 2017). Thus, garnet has a different metasomatic origin from that in Hannuoba garnet pyroxenite. The later uplift and melt percolation caused growth of garnet and spinel coevally at the garnet-spinel transition in the pyroxenite field (Figs. 2 and 3; Johanesen et al., 2014). Because the deeper units remained warmer at this point, the garnet begin to breakdown. On the other hand, the mantle and core of the kelyphite have nearly the same bulk chemical composition as the precursor garnet, whereas the rim of the kelyphites have higher FeO, MgO and lower CaO than the mantle and core (Table 2). The transition between the kelyphite rim and clinopyroxene is gradual, indicating that the kelyphite rim of garnet could be attributed to the following simplified reaction during decompression: garnet + clinopyroxene = orthopyroxene + spinel + plagioclase (Kushiro and Yoder Jr., 1966; Thompson, 1979). The temperature at which this reaction took place has been estimated to be 800 ± 50 °C, upon a further decompression (Obata, 2011, Obata et al., 2013).

5.3. Protolith of the Jiande clinopyroxenite xenolith

The clinopyroxenite xenoliths in Jiande show granuloblastic metamorphic texture and consist of clinopyroxene, partially to completely kelyphitized garnet, and spinel with minor amounts of sapphirine and plagioclase (Figs. 2 and 3). The occurrence of sapphirine, which always surrounds spinel, suggests their formation during the cooling/uplift process. The isochemical kelyphite usually encloses primitive spinel, indicating primary garnet would be formed at the expense of spinel at the garnet-spinel transition. Thus, microtextural and reaction relationships suggest that the mineral assemblage at the earliest metamorphic conditions in these xenoliths was clinopyroxene and spinel.

Obata et al. (2006) demonstrated that cumulus gabbros which originally precipitated from basaltic magmas at low pressure are characterized by a clear linear trend between Al_2O_3/MgO and SiO_2/MgO. The Jiande clinopyroxenite xenoliths do not define a linear correlation (Fig. 5a). Furthermore, the clinopyroxene and garnet do not have positive Eu anomalies that are typical for oceanic gabbros (Fig. 7; Jacob, 2004; Morishita et al., 2003). In addition, the Li content of clinopyroxene in eclogitic rocks occurring in a variety of geologic settings has been used to provide constraints on the origin of these rocks (Woodland et al., 2002). Metabasaltic (metagabbroic) eclogites from high-pressure terranes have high Li contents, whereas all kimberlite- and basanite-hosted xenoliths representing high-pressure cumulates have low Li contents (Fig. 8a; Woodland et al., 2002). The clinopyroxenes in the Jiande clinopyroxenite xenoliths have Li abundances similar to high-P mafic cumulate but much lower than those in the Hannuoba and Ronda pyroxenites, and crustal eclogite (Fig. 8a; Morishita et al., 2009; Woodland et al., 2002). These features suggest that the Jiande clinopyroxenite xenolith is not a plagioclase-rich, low-pressure cumulate (Morishita et al., 2001, 2003, 2009), but is most likely a pyroxenite, originating as clinopyroxene + spinel cumulate from mafic melts percolating through the mantle. However, upon further ascent and melt percolation, the garnet/kelyphite and sapphirine occurred. The earlier compositions of clinopyroxene and spinel change due to re-equilibration with metamorphic minerals.

5.4. P-T path for the Jiande clinopyroxenite xenolith

As noted above, the earliest metamorphic mineral assemblages were characterized by clinopyroxene + spinel. Temperature and pressure at which the earliest mineral assemblages were equilibrated is difficult to estimate from mineral compositions using geothermometers because the minerals were significantly affected by chemical re-equilibration.

Reaction textures, such as garnet and sapphirine formation, kelyphitization of garnet followed by disappearance of garnet, were formed during decompression processes. Since most kelyphites have chemical composition similar to relic garnets, three different garnet-clinopyroxene thermometer for garnet pyroxenite could be used to calculate the latest T condition (Dahl, 1980; Krogh, 1988; Powell, 1985). The calculated temperatures for the Jiande clinopyroxenite xenoliths fall within the ranges of 967–1138 °C (Table 5). The occurrence of sapphirine could also provide an additional P-T mineral estimates (Christy, 1989; Sato et al., 2006; Su et al., 2012). Sapphirine has a limited stability field in mantle conditions of about 8–10 kbar spinel pyroxenite stability field, corresponding to the crust-mantle boundary (Su et al., 2012). At this pressure, the sapphirine-spinel geothermometer gave temperatures of 1069–1094 °C (Sato et al., 2006), overlapping with the estimates using garnet-clinopyroxene thermometer. Thus, we concluded that the latest P-T condition recorded in the Jiande clinopyroxenite xenoliths was at P = 8–10 GPa and T = 1069–1094 °C.

Cenozoic Jiande basalts host abundant peridotite xenoliths and minor pyroxenite. Pressure recorded in the Jiande lherzolites is at 15 kbar (~51 km; Hao et al., 2014). If this pressure estimate is valid, it implies that these clinopyroxenite xenoliths may originated from similar levels. This pressure condition is higher than the stability field of sapphirine formation (8–10 kbar). Therefore, these xenoliths were tectonically emplaced at shallow levels before being entrained in the host magmas due to the uplift of the lithospheric mantle.

Eastern China has been strongly affected by the subduction of the Pacific Plate (Sun et al., 2007). The lithospheric thinning process occurred and accompanied the extension of the lithosphere and upwelling of the asthenosphere (Fan et al., 2000; Griffin et al., 1998; Liu et al., 2012, 2017; Lu et al., 2013, 2015; Xu et al., 2000, 2003; Yu et al., 2003; Zheng et al., 2001, 2004). It is therefore possible that the Jiande clinopyroxenite xenoliths were probably lifted during this episode.

6. Conclusions

The occurrence of rare sapphirine- and garnet-bearing clinopyroxenite xenolith coexisting with abundances of spinel lherzolites entrained in the Jiande basalts provides an insight into their petrogenesis and metamorphic history of the crust-mantle transition region. Spinel and clinopyroxene are the main phases in the Jiande clinopyroxenite xenoliths. Reaction textures, such as sapphirine formation, kelyphitization of garnet followed by disappearance of the garnet, were formed during decompression. The latest P-T conditions recorded by the occurrence of sapphirine in the Jiande clinopyroxenite xenoliths were at P = 8–10 GPa and T = 1069–1094 °C. The equilibrium pressure estimated by coexisted lherzolites is at 15 kbar, representing the estimate for the formation of spinel + clinopyroxene at mantle depth. Therefore, these clinopyroxenite xenoliths were tectonically emplaced at shallow levels before being entrained in the host magmas due to the uplift of the lithospheric mantle.

Acknowledgements

We would like to thank Di Zhang, Qian Mao and Yu-Guang Ma for their assistance with the electron microprobe analyses, and Guo-Qiang Tang, Xiao-Xiao Ling and Jiao Li for the SIMS analyses. Many thanks to Johnnie Chamberlin and Chen Chen for comments on the early version of the manuscript. Constructive and detailed comments from Tomoaki Morishita are greatly appreciated. Marina Koreshkova and another

anonymous reviewer are warmly acknowledged for their careful and constructive reviews, which considerably improved this paper. This study was supported by the National Natural Science Foundation of China (Grants 41673037 and 41273020) and Youth Innovation Promotion Association, Chinese Academy of Sciences (Grant 2017095).

References

Ackermand, D., Seifert, F., Schreyer, W., 1975. Instability of sapphirine at high pressures. Contributions to Mineralogy and Petrology 50, 79–92.

Anders, E., Grevesse, N., 1989. Abundances of the elements: meteoritic and solar. Geochimica et Cosmochimica Acta 53, 197–214.

Arima, M., Barnett, R.L., 1984. Sapphirine bearing granulites from the Sipiwesk Lake area of the late Archean Pikwitonei granulite terrain, Manitoba, Canada. Contributions to Mineralogy and Petrology 88, 102–112.

Bilal, A., 2016. Sapphirine and fluid inclusions in Tel Thanoun mantle xenoliths, Syria. Journal of African Earth Sciences 116, 105–113.

Christy, A.G., 1989. The stability of sapphirine + clinopyroxene: implications for phase relations in the CaO-MgO-Al_2O_3-SiO_2 system under deep-crustal and upper mantle conditions. Contributions to Mineralogy and Petrology 102, 422–428.

Dahl, P.S., 1980. The thermal-compositional dependence of Fe^{2+}-Mg distributions between coexisting garnet and pyroxene: applications to geothermometry. American Mineralogist 65, 852–866.

Fan, W.M., Zhang, H.F., Baker, J., Jarvis, K.E., Mason, P.R.D., Menzies, M.A., 2000. On and off the North China Craton: where is the Archaean keel? Journal of Petrology 41, 933–950.

Galli, A., Le Rayon, B., Schmidt, M.W., Burg, J.P., Caddick, M.J., Reusser, E., 2011. Granulites and charnockites of the Gruf complex: evidence for permian ultra-high temperature metamorphism in the Central Alps. Lithos 124, 17–45.

Giovanardi, T., Morishita, T., Zanetti, A., Mazzucchelli, M., Vannucci, R., 2013. Igneous sapphirine as a product of melt-peridotite interactions in the Finero Phlogopite-Peridotite Massif, Western Italian Alps. European Journal of Mineralogy 25, 17–31.

Gregoire, M., Jackson, I., O'Reilly, S.Y., Cottin, J.Y., 2001. The lithospheric mantle beneath the Kerguelen Islands (Indian Ocean): petrological and petrophysical characteristics of mantle mafic rock types and correlation with seismic profiles. Contributions to Mineralogy and Petrology 142, 244–259.

Griffin, W.L., O'Reilly, S.Y., 1986. Mantle-derived sapphirine. Mineralogical Magazine 50, 635–640.

Griffin, W.L., Andi, Z., O'Reilly, S.Y., Ryan, C.G., 1998. Phanerozoic evolution of the lithosphere beneath the Sino-Korean Craton. In: Flower, M.F.J., Chung, S.L., Lo, C.H., Lee, T.Y. (Eds.), Mantle Dynamics and Plate Interactions in East Asia. American Geophysical Union, Washington D.C., pp. 107–126.

Hao, Y.T., Xia, Q.K., Li, Q.W., Chen, H., Feng, M., 2014. Partial melting control of water contents in the Cenozoic lithospheric mantle of the Cathaysia block of South China. Chemical Geology 380, 7–19.

Ho, K.S., Chen, J.C., Lo, C.H., Zhao, H.L., 2003. ^{40}Ar-^{39}Ar dating and geochemical characteristics of late Cenozoic basaltic rocks from the Zhejiang-Fujian region, SE China: eruption ages, magma evolution and petrogenesis. Chemical Geology 197, 287–318.

Hu, Y., Teng, F.Z., Zhang, H.F., Xiao, Y., Su, B.X., 2016. Metasomatism-induced mantle magnesium isotopic heterogeneity: evidence from pyroxenites. Geochimica et Cosmochimica Acta. https://doi.org/10.1016/j.gca.2015.11.001.

Huang, X.L., Xu, Y.G., 2010. Thermal state and structure of the lithosphere beneath eastern China: a synthesis on basalt-borne xenoliths. Journal of Earth Science 21, 711–730.

Huang, X.L., Xu, Y.G., Liu, D.Y., 2004. Geochronology, petrology and geochemistry of the granulite xenoliths from Nvshan, East China: implication for a heterogeneous lower crust beneath the Sino-Korean Craton. Geochimica et Cosmochimica Acta 68, 127–149.

Jacob, D., 2004. Nature and origin of eclogite xenoliths from kimberlites. Lithos 77, 295–316.

Jiao, S.J., Guo, J.H., 2011. Application of the two-feldspar geothermometer to ultrahigh-temperature (UHT) rocks in the khondalite belt, North China craton and its implications. American Mineralogist 96, 250–260.

Jiao, S.J., Guo, J.H., Wang, L.J., Peng, P., 2015. Short-lived high-temperature prograde and retrograde metamorphism in Shaerqin sapphirine-bearing metapelites from the Daqingshan terrane, North China Craton. Precambrian Research 269, 31–57.

Johanesen, K., Platt, J.P., Kaplan, M.S., Ianno, A.J., 2014. A revised thermal history of the Ronda peridotite, S. Spain: new evidence for excision during exhumation. Earth and Planetary Science Letters 393, 187–199.

Kornprobst, J., Piboule, M., Roden, M., Tabit, A., 1990. Corundum-bearing garnet clinopyroxenites at Beni Bousera (Morocco): original plagioclase-rich gabbros recrystallized at depth within the mantle? Journal of Petrology 31, 717–745.

Krogh, E.J., 1988. The garnet-clinopyroxene Fe-Mg geothermometer - a reinterpretation of existing experimental data. Contributions to Mineralogy and Petrology 99, 44–48.

Kushiro, I., Yoder Jr., H.S., 1966. Anorthite-forsterite and anorthite-enstatite reactions and their bearing on the basalt-eclogite transformation. Journal of Petrology 7, 337–362.

Lal, R.K., 1997. Internally consistent calibrations for geothermobarometry of high-grade Mg-Al rich rocks in the system MgO-Al_2O_3-SiO_2 and their application to sapphirine-spinel granulites of Eastern Ghats, India and Enderby Land, Antarctica. Proceedings of the Indian Academy of Sciences 106, 91–113.

Lal, R.K., Ackermand, D., Upadhyay, H., 1987. P-T-X relationship deduced from corona textures in sapphirine-spinel-quartz assemblages from Paderu, Southern India. Journal of Petrology 28, 1139–1168.

Li, X.H., Li, Z.X., He, B., Li, W.X., Li, Q.L., Gao, Y.Y., Wang, X.C., 2012. The Early Permian active continental margin and crustal growth of the Cathaysia Block: in situ U-Pb, Lu-Hf and O isotope analyses of detrital zircons. Chemical Geology 328, 195–207.

Li, X.H., Li, Z.X., Li, W.X., 2014. Detrital zircon U-Pb age and Hf isotope constrains on the generation and reworking of Precambrian continental crust in the Cathaysia Block, South China: a synthesis. Gondwana Research 25, 1202–1215.

Liu, Y.S., Gao, S., Lee, C.T.A., Hu, S.H., Liu, X.M., Yuan, H.L., 2005. Melt–peridotite interactions: links between garnet pyroxenite and high-Mg# signature of continental crust. Earth and Planetary Science Letters 234, 39–57.

Liu, Y.S., Hu, Z.C., Gao, S., Günther, D., Xu, J., Gao, C.G., Chen, H.H., 2008. In situ analysis of major and trace elements of anhydrous minerals by LA-ICP-MS without applying an internal standard. Chemical Geology 257, 34–43.

Liu, R., Zhou, H., Zhang, L., Zhong, Z., Zeng, W., Xiang, H., et al., 2009. Paleoproterozoic reworking of ancient crust in the Cathaysia Block, South China: evidence from zircon trace elements, U-Pb and Lu-Hf isotopes. Chinese Science Bulletin 54, 1543–1554.

Liu, C.Z., Wu, F.Y., Sun, J., Chu, Z.Y., Qiu, Z.L., 2012. The Xinchang peridotite xenoliths reveal mantle replacement in southeastern China. Lithos 150, 171–187.

Liu, C.Z., Zhang, C., Liu, Z.C., Sun, J., Chu, Z.Y., Qiu, Z.L., Wu, F.Y., 2017. Formation age and metasomatism of the sub-continental lithospheric mantle beneath southeast China: Sr-Nd-Hf-Os isotopes of Mingxi mantle xenoliths. Journal of Asian Earth Sciences 145, 591–604.

Lu, J.G., Zheng, J.P., Griffin, W.L., Yu, C.M., 2013. Petrology and geochemistry of peridotite xenoliths from the Lianshan region: nature and evolution of lithospheric mantle beneath the lower Yangtze block. Gondwana Research 23, 161–175.

Lu, J.G., Zheng, J.P., Griffin, W.L., O'Reilly, S.Y., Pearson, N.J., 2015. Microscale effects of melt infiltration into the lithospheric mantle: peridotite xenoliths from Xilong, South China. Lithos 232, 111–123.

McDonough, W.F., Sun, S.S., 1995. The composition of the Earth. Chemical Geology 120, 223–253.

Meyer, H.O.A., Brookins, D.G., 1976. Sapphirine, sillimanite, and garnet in granulite xenoliths from Stockdale kimberlite, Kansas. American Mineralogist 61, 1194–1202.

Morimoto, N., 1989. Nomenclature of pyroxenes. Subcommittee of new minerals and mineral names. Canadian Mineralogist 27, 143–156.

Morishita, T., Arai, S., Gervilla, F., 2001. High-pressure aluminous mafic rocks from the Ronda peridotite massif, southern Spain: significance of sapphirine-and corundum-bearing mineral assemblages. Lithos 57, 143–161.

Morishita, T., Arai, S., Gervilla, F., Green, D.H., 2003. Closed-system geochemical recycling of crustal materials in alpine-type peridotite. Geochimica et Cosmochimica Acta 67, 303–310.

Morishita, T., Arai, S., Ishida, Y., Tamura, A., Gervilla, F., 2009. Constraints on the evolutionary history of aluminous mafic rocks in the Ronda peridotite massif (Spain) from trace-element compositions of clinopyroxene and garnet. Geochemical Journal 43, 191–206.

Naemura, K., Hirajima, T., Svojtka, M., 2009. The pressure-temperature path and the origin of phlogopite in spinel-garnet peridotites from the Blansky Les Massif of the Moldanubian Zone, Czech Republic. Journal of Petrology 50, 1795–1827.

Obata, M., 2011. Kelyphite and symplectite: textural and mineralogical diversities and universality, and a new dynamic view of their structural formation. New Frontiers in Tectonic Research - General Problems, Sedimentary Basins and Island Arcs, pp. 93–122.

Obata, M., Hirajima, T., Svojtka, M., 2006. Origin of eclogite and garnet pyroxenite from the Moldanubian Zone of the Bohemian Massif, Czech Republic and its implication to other mafic layers embeded in orogenic peridotites. Mineralogy and Petrology 88, 321–340.

Obata, M., Ozawa, K., Naemura, K., Miyake, A., 2013. Isochemical breakdown of garnet in orogenic garnet peridotite and its implication to reaction kinetics. Mineralogy and Petrology 107, 881–895.

Okay, A.I., 1994. Sapphirine and Ti-clinohumite in ultra-high-pressure garnet-pyroxenite and eclogite from Dabie Shan, China. Contributions to Mineralogy and Petrology 116, 145–155.

Powell, R., 1985. Regression diagnostic and robust regression in geothermometer/geobarometer calibration: the garnet-clinopyroxene geothermometer revisited. Journal of Metamorphic Geology 3, 231–243.

Santosh, M., Tsunogae, T., Li, J.H., Liu, S.J., 2007. Discovery of sapphirine bearing Mg-Al granulites in the North China Craton: implications for Paleopro-terozoic ultrahigh temperature metamorphism. Gondwana Research 11, 263–285.

Santosh, M., Sajeev, K., Li, J.H., Liu, S.J., Itaya, T., 2009. Counterclockwise ex-humation of a hot orogen: the Paleoproterozoic ultrahigh-temperature granulites in the North China Craton. Lithos 110, 140–152.

Sato, K., Miyamoto, T., Kawasaki, T., 2006. Experimental calibration of sapphirine–spinel Fe^{2+}–Mg exchange thermometer: implication for constraints on P–T condition of Howard Hills, Napier Complex, East Antarctica. Gondwana Research 9, 398–408.

Sobolev, N.V., Lavrent'ev, Y.G., Pokhilenko, N.P., Usova, L.V., 1973. Chrome-rich garnets from the kimberlites of Yakutia and their parageneses. Contributions to Mineralogy and Petrology 40, 39–52.

Su, B.X., Zhang, H.F., Hu, Y., Santosh, M., Tang, Y.J., Xiao, Y., 2012. The genesis of mantle-derived sapphirine. American Mineralogist 97, 856–863.

Su, B.X., Zhang, H.F., Deloule, E., Vigier, N., Hu, Y., Tang, Y.J., Xiao, Y., Sakyi, P.A., 2014. Distinguishing silicate and carbonatite mantle metasomatism by using lithium and its isotopes. Chemical Geology 381, 67–77.

Su, B.X., Gu, X.Y., Deloule, E., Zhang, H.F., Li, Q.L., Li, X.H., Vigier, N., Tang, Y.J., Tang, G.Q., Liu, Y., Pang, K.N., Brewer, A., Mao, Q., Ma, Y.G., 2015. Potential orthopyroxene, clinopyroxene and olivine reference materials for in situ lithium isotope determination. Geostandards and Geoanalytical Research 39, 357–369.

Sun, W.D., Ding, X., Hu, Y.H., Li, X.H., 2007. The golden transformation of the Cretaceous plate subduction in the west Pacific. Earth and Planetary Science Letters 262, 533–542.

Sutherland, F.L., Coenraads, R.R., Schwarz, D., Raynor, L.R., Barron, B.J., Webb, G.B., 2003. Al-rich diopside in alluvial ruby and corundum-bearing xenoliths, Australian and SE Asian basalt fields. Mineralogical Magazine 67, 717–732.

Thompson, A.B., 1979. Metamorphism in a model mantle: I. Predictions of P-T-X relations in CaO-Al_2O_3-MgO-SiO_2. In: Boyd, F.R., Meyer, H.O.A. (Eds.), The Mantle Samples: Inclusions in Kimberlites and Other Volcanics. Proceedings of the Second International Kimberlite Conference vol. 2. American Geophysical Union, Washington, D.C., pp. 15–28.

Tomascak, P.B., Langmuir, C.H., le Roux, P.J., Shirey, S.B., 2008. Lithium isotopes in global mid-ocean ridge basalts. Geochimica et Cosmochimica Acta 72, 1626–1637.

Woodland, A.B., Seitz, H.M., Altherr, R., Marschall, H., Olker, B., Ludwig, T., 2002. Li abundances in eclogite minerals: a clue to a crustal or mantle origin? Contributions to Mineralogy and Petrology 143, 587–601.

Xia, Y., Xu, X.S., Zhu, K.Y., 2012. Paleoproterozoic S- and A-type granites in southwestern Zhejiang: magmatism, metamorphism and implications for the crustal evolution of the Cathaysia basement. Precambrian Research 216-219, 177–207.

Xiao, Y., Zhang, H.F., Su, B.X., Zhu, B., Chen, B.B., Chen, C., Sakyi, P.A., 2017. Partial melting control of lithium concentrations and isotopes in the Cenozoic lithospheric mantle beneath Jiande area, the Cathaysia block of SE China. Chemical Geology 466, 750–761.

Xu, X.S., O'Reily, S.Y., Zhou, X.M., Griffin, W.L., 1996. A xenolith-derived geotherm mad the crust mantle boundary at Qilin, southeastern China. Lithos 38, 41–62.

Xu, X.S., O'Reilly, S.Y., Griffin, W.L., Zhou, X.M., 2000. Genesis of young lithospheric mantle in SE China. Journal of Petrology 41, 111–148.

Xu, X.S., O'Reilly, S.Y., Griffin, W.L., Zhou, X.M., 2003. Enrichment of upper mantle peridotite: petrological, trace element and isotopic evidence in xenoliths from SE China. Chemical Geology 198, 163–188.

Yu, J.H., Fang, Z., Zhou, X., Lai, M., Xu, X., 1998. Garnet granulite facies xenoliths from Yingfengling Cenozoic basalt in Leizhou, Guangdong Province. Chinese Science Bulletin 43, 2013–2018.

Yu, J.H., O'Reilly, S.Y., Griffin, W.L., Xu, X.S., Zhang, M., Zhou, X.M., 2003. The thermal state and composition of the Lithospheric Mantle beneath the Leizhou Peninsula South China. Journal of Volcanology and Geothermal Research 122, 165–189.

Yu, J.H., O'Reilly, S.Y., Wang, L.J., Griffin, W.L., Zhou, M.F., Zhang, M., et al., 2010. Components and episodic growth of Precambrian crust in the Cathaysia Block, South China: evidence from U-Pb ages and Hf isotopes of zircons in Neoproterozoic sediments. Precambrian Research 181, 97–114.

Zhang, R.Y., Cong, B.L., 1987. Cenozoic volcanic rocks and the ultramafic xenoliths in south eastern China. In: E, M. L., Zhao, D.S. (Eds.), Cenozoic Basalts and the Deep-seated Rock Xenoliths in Eastern China. Science Publication House, Beijing, pp. 349–467 (In Chinese).

Zhang, H.F., Deloule, E., Tang, Y.J., Ying, J.F., 2010. Melt/rock interaction in remains of refertilized Archean lithospheric mantle in Jiaodong Peninsula, North China Craton: Li isotopic evidence. Contributions to Mineralogy and Petrology 160, 261–277.

Zhao, X.M., Cao, H.H., Mi, X., Evans, N.J., Qi, Y.H., Huang, F., Zhang, H.F., 2017. Combined iron and magnesium isotope geochemistry of pyroxenite xenoliths from Hannuoba, North China Craton: implications for mantle metasomatism. Contributions to Mineralogy and Petrology 172, 40.

Zheng, J.P., O'Reilly, S.Y., Griffin, W.L., Lu, F.X., Zhang, M., Pearson, N.J., 2001. Relict refractory mantle beneath the eastern North China block: significance for lithosphere evolution. Lithos 57, 43–66.

Zheng, J.P., O'Reilly, S.Y., Griffin, W.L., Zhang, M., Lu, F.X., Liu, G.L., 2004. Nature and evolution of Mesozoic-Cenozoic lithospheric mantle beneath the Cathaysia block, SE China. Lithos 74, 41–65.